

Intra-beam Scattering Theory and RHIC Experiments

J. Wei, A. Fedotov, W. Fischer, N. Malitsky, G. Parzen* and J. Qiang[†]

*Brookhaven National Laboratory, Upton, New York 11973, USA ¹

[†]Lawrence Berkeley National Laboratory, California 29720, USA

Abstract. Intra-beam scattering is the leading mechanism limiting the luminosity in heavy-ion storage rings like the Relativistic Heavy Ion Collider (RHIC). The multiple Coulomb scattering among the charged particles causes transverse emittance growth and longitudinal beam de-bunching and beam loss, compromising machine performance during collision. Theoretically, the original theories developed by Piwinski [1], Bjorken, and Mtingwa [2] only describe the rms beam size growth of an unbounded Gaussian distribution. Equations based on the Fokker-Planck approach are developed to further describe the beam density profile evolution and beam loss [3, 4, 5]. During the 2004 RHIC heavy-ion operation, dedicated IBS experiments were performed to bench-mark the rms beam size growth, beam loss, and profile evolution both for a Gaussian-like and a longitudinal hollow beam. This paper summarizes the IBS theory and discusses the experimental bench-marking results.

INTRODUCTION

Since three decades ago, intra-beam Coulomb scattering (IBS) has been recognized as a mechanism that degrades the quality of high-brightness hadron beams in storage rings [1]. The scattering cross section is a strong function of the charge state of the particles. For heavy ion colliders like RHIC, IBS plays a leading role limiting the luminosity.

At the top energy for beam storage, the luminosity deteriorates due to the growth of the horizontal emittance that is coupled through dispersion to IBS-induced momentum growth, to the growth of the vertical emittance that is transversely coupled to the horizontal growth, and to the reduction of beam intensity when particles are driven out of the RF buckets by the diffusion process. The IBS-induced particle loss contributes to the experimental background that demands beam collimation and cleaning during the nominal 10-hour storage.

IBS also complicates the RHIC operation at injection. At a low energy below the transition energy, IBS causes fast growth in the momentum spread. The two rings need to be filled quickly in several minutes to avoid longitudinal phase-space dilution that can complicate transition crossing and top-energy RF recapture.

IBS effects predicted previously during the RHIC design have all been confirmed during the operations in recent years [7, 3]. As shown in Fig. 1, during a typical 5-hour store at the top energy of 100 GeV/u, about 40% of the gold beam escapes the RF bucket. The unbunched beam also fills the abort gap, which needs to be free of particles to avoid quenches when the beam is dumped.

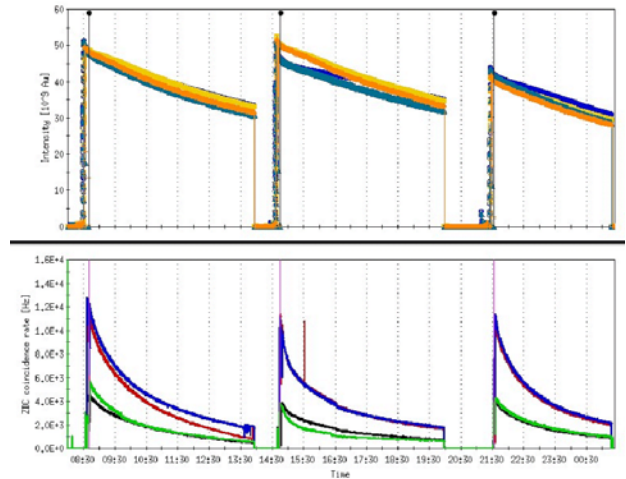


FIGURE 1. Reduction of beam intensity in the blue and yellow ring (top) and luminosity degradation measured at different interaction point (bottom) of the $^{197}\text{Au}^{79+}$ beam during a 5-hour store in RHIC.

Combined with the transverse emittance growth, the luminosity lifetime is about two hours.

IBS effects in hadron storage rings can be mitigated by beam cooling methods like stochastic and electron cooling [8, 9].

This paper attempts to summarize the theories developed on IBS, and presents experimental bench-marking results from RHIC. We first describe the IBS mechanism using the beam rest-frame Hamiltonian. Then, we present IBS theories on the beam size growth and density distribution evolution. Year 2004 beam-experiment results in RHIC are compared with theoretical predictions including rms beam size growths, de-bunching beam loss, and longitudinal profile evolution during RHIC storage. Discussions and a summary are given in the end.

¹ Work performed under the auspices of the U.S. Department of Energy.

MECHANISM

IBS refers to two-body, small-angle multiple Coulomb scattering processes that occurs between the particles in the same circulating bunch [1, 2, 6, 7]. Energy exchanges and temperature increases in the particle rest-frame manifest themselves as variations in the beam's emittance and momentum spread in the laboratory frame [10].

IBS mechanism can be described using the rest frame (x, y, z, t) of the circulating synchronous particle. Measure dimensions in units of the characteristic distance ξ_0 with $\xi_0^3 = r_0 \rho^2 / \beta^2 \gamma^2$, time in units of $\rho / \beta \gamma c$, and energy in units of $\beta^2 \gamma^2 Z^2 e^2 / 4\pi \epsilon_0 \xi_0$, where $r_0 = Z^2 e^2 / 4\pi \epsilon_0 m_0 c^2$ is the classical radius, βc and $\gamma m_0 c^2$ are the velocity and energy of the synchronous particle, and ρ is the radius of curvature in bending regions of magnetic field B_0 . The Hamiltonian for particles in a simple system with bending dipoles and focusing quadrupoles of strength $n_1 = -(\rho/B_0)(\partial B_y/\partial x)$ is [11]

$$H = \begin{cases} \frac{P_x^2 + P_y^2 + P_z^2}{2} + \frac{x^2}{2} - \gamma x P_z + V_C & \text{(bend)} \\ \frac{P_x^2 + P_y^2 + P_z^2}{2} - \frac{n_1(x^2 - y^2)}{2} + V_C + U_s & \text{(straight)} \end{cases} \quad (1)$$

where U_z is the potential provided by the RF system. The Coulomb potential is non-relativistic in the rest frame:

$$V_C = \sum_j \frac{1}{\sqrt{(x_j - x)^2 + (y_j - y)^2 + (z_j - z)^2}}. \quad (2)$$

In terms of dispersion function D and betatron displacements $\beta_{x,y}$, this Hamiltonian is transformed to

$$\bar{H} = \frac{P_{\beta_x}^2 + P_{\beta_y}^2}{2} + \frac{1 - \gamma^2 F_z}{2} P_z^2 + V_C + U_z, \quad (3)$$

where

$$F_z = \begin{cases} D + DD' + (D')^2 & \text{(bend)} \\ DD'' + (D')^2 & \text{(straight)} \end{cases} \quad (4)$$

and

$$\langle F_z \rangle = \frac{1}{\gamma_T^2}. \quad (5)$$

Below transition energy, $\gamma < \gamma_T$, particles are in a positive-mass regime. In an idealized case that the machine lattice is uniform along the ring circumference, the Hamiltonian in the rest frame is time-independent. The particle system is thus closed, and the total kinetic energy (or temperature) is bounded. The heat can be transferred from the high temperature to the low temperature direction. The system eventually reaches an equilibrium state when the temperature (i.e. rest-frame velocity) is the same in all directions.

In an actual alternating-gradient focusing ring, the beam sees a time dependent potential modulated by

the ring lattice frequency. The beam structure absorbs "phonons" and heats up [10]. Intra-beam multiple scattering manifests as a mixture of thermal equalization and temperature growth asymptotically approaching equal temperature in all directions in the rest frame.

Above transition energy, $\gamma > \gamma_T$, the beam is in a negative-mass regime. The Hamiltonian (Eq. 3) indicates that even in the case of a uniform machine lattice, beam temperature can grow simultaneously in the longitudinal and transverse directions.

THEORY

In general, evaluation of IBS processes consists of calculating the scattering rate in the rest frame of the circulating particle based on the Rutherford scattering cross section, transformation to the laboratory frame, and averaging over phase-space and time.

Gaussian-beam rms growth

In the laboratory frame, the rate of emittance and momentum growth is obtained [1, 2] assuming multiple small-angle scattering among particles with Gaussian distribution in the six-dimensional phase space. In the case that $D/\beta_x^{1/2}$ is nearly constant (e.g. for FODO lattice), the growth rate formula can be simplified as [7, 12]

$$\begin{bmatrix} \frac{1}{\sigma_p} \frac{d\sigma_p}{dt} \\ \frac{1}{\sigma_x} \frac{d\sigma_x}{dt} \\ \frac{1}{\sigma_y} \frac{d\sigma_y}{dt} \end{bmatrix} = \frac{q^4 N r_0^2 m_0 c^2 L_C F(\chi)}{A^2 8\gamma \epsilon_{N_x} \epsilon_{N_y} S_{rms}} \begin{bmatrix} n_b(1-d^2) \\ -a^2/2 + d^2 \\ -b^2/2 \end{bmatrix}, \quad (6)$$

where $L_C \approx 20$ is the Coulomb logarithm, $\epsilon_{N_{x,y}} = \beta \gamma \sigma_{x,y}^2 / \beta_{x,y}$ is the normalized rms transverse emittance, $S_{rms} = \pi m_0 c^2 \beta \gamma \sigma_s \sigma_p / cA$ is the rms longitudinal bunch area in phase space, $\chi = (a^2 + b^2)/2$, $d = \frac{D\sigma_p}{(\sigma_x^2 + D^2\sigma_p^2)^{1/2}}$, $a = \frac{\beta_x d}{D\gamma}$, $b = \frac{\beta_y \sigma_x}{\beta_x \sigma_y} a$, n_b is equal to 1 if the beam is longitudinally bunched, and is equal to 2 if it is not. For the bunched beams, σ_s is the rms bunch length and N is the number of particles per bunch; for unbunched beams, N is the total number of particles and $\sigma_s = \sqrt{\pi} R_0$. In Eq. 6, $F(\chi)$ is an analytic function given by

$$F(\chi) = \frac{-3 + (1 + 2\chi)I(\chi)}{1 - \chi}, \quad (7)$$

where

$$I(\chi) = \begin{cases} \frac{1}{\sqrt{\chi(\chi-1)}} \text{Arth} \sqrt{\frac{\chi-1}{\chi}} & \chi \geq 1; \\ \frac{1}{\sqrt{\chi(1-\chi)}} \arctan \sqrt{\frac{1-\chi}{\chi}} & \chi < 1. \end{cases} \quad (8)$$

The growth rates are linearly proportional to the bunch intensity N , and are strongly dependent ($\sim Z^4/A^2$) on the charge state of the particle. Except for the form factors χ , d , a , and b that depend on the ratio of the beam amplitudes in different dimension, the rates are inversely proportional to the six dimensional phase space area.

Below transition energy, the asymptotic distribution corresponds to the condition

$$\left\langle \frac{\sigma_x}{\beta_x} \right\rangle \approx \left\langle \frac{\sigma_y}{\beta_y} \right\rangle \approx \frac{\sigma_p}{\gamma}, \quad \gamma \ll \gamma_T.$$

Above transition energy, the asymptotic distribution corresponds to the condition

$$\sqrt{n_b n_c} \langle \sigma_x \rangle \approx \langle D \rangle \sigma_p, \quad \gamma \gg \gamma_T$$

where n_c is equal to 1 if the horizontal and vertical motion are uncoupled, and is equal to 2 if they are fully coupled. Coupling between the horizontal and vertical motion helps reducing the horizontal growth. In such a case, the growth rates at energies far above transition are

$$\left[\begin{array}{c} \frac{1}{\sigma_p} \frac{d\sigma_p}{dt} \\ \frac{1}{\sigma_x} \frac{d\sigma_x}{dt} \end{array} \right] = \frac{Z^4 N}{A^2} \frac{\pi r_0^2 m_0 c^2 L_c}{16 \gamma_T \epsilon_x \epsilon_y S_{rms}} \left[\begin{array}{c} n_b (1-d^2)/d \\ d/n_c \end{array} \right], \quad (9)$$

which is approximately independent of the beam energy.

Fokker-Planck approach on distribution

The conventional theory based on unbounded Gaussian distribution [1, 2] is inadequate in evaluating beam intensity and luminosity lifetime. Instead, we use the Fokker-Planck equation to describe the evolution of particle distribution in the phase space. The general 6 dimensional (6-D) equation can be greatly simplified by the fact that the IBS growth time is typically much longer than the synchrotron-oscillation period, which is again much longer than the multiple collision relaxation time. For the case of RHIC, the leading source of beam loss is in the longitudinal direction due to the limited RF voltage. We further assume in the transverse directions a time-evolving Gaussian distribution. After averaging over the machine circumference and the synchrotron phase for all the particles involved in the collision [3], we obtain a 1-D Fokker-Planck equation of the density function $\Psi(J)$ in the longitudinal direction in terms of the action variable J ,

$$\frac{\partial \Psi}{\partial t} = -\frac{\partial}{\partial J} (F\Psi) + \frac{1}{2} \frac{\partial}{\partial J} \left(D \frac{\partial \Psi}{\partial J} \right), \quad (10)$$

with the boundary conditions

$$\left\{ \begin{array}{l} J = 0: \quad -F\Psi + \frac{D}{2} \frac{\partial \Psi}{\partial J} = 0, \\ J = J_{max}: \quad \Psi = 0. \end{array} \right. \quad (11)$$

Here, the dynamical drift coefficient $F(J)$ is given by

$$F = \oint \frac{2ds}{\pi R} \int_0^{\frac{1}{4}} dQ \left. \frac{\partial W}{\partial J} \right|_{\phi}^{-1} (Q, J) \int_{J_{min}}^J \left. \frac{\partial W}{\partial J} \right|_{\phi} (Q', J') [A_F(\lambda_1) + A_F(\lambda_2)] \Psi(J') dJ' \quad (12)$$

and the diffusion coefficient $D(J)$ is given by

$$D = \oint \frac{2ds}{\pi R} \int_0^{\frac{1}{4}} dQ \left[\left. \frac{\partial W}{\partial J} \right|_{\phi}^{-1} (Q, J) \right]^2 \int_{J_{min}}^J \left. \frac{\partial W}{\partial J} \right|_{\phi} (Q', J') [A_D(\lambda_1) + A_D(\lambda_2)] \Psi(J') dJ' \quad (13)$$

where

$$A_F(\lambda) = -\frac{2Z^4 r_0^2 L_c E}{A^2 \beta^2 \gamma^4} \frac{I_F(\lambda)}{\sigma_x \sigma_y}, \quad A_D(\lambda) = \frac{Z^4 r_0^2 L_c E^2}{A^2 \gamma^3 h \omega_s} \frac{I_D(\lambda)}{\sigma_x \sigma_y}, \quad (14)$$

$\lambda_{1,2} = \frac{h\omega_s g}{\gamma \beta^2 E} (W \mp W')$, $g = \frac{1}{2} \sqrt{\frac{\beta \gamma \beta_{x,y}}{\epsilon_{x,y}}}$, ω_s is the revolution frequency,

$$\left. \frac{\partial W}{\partial J} \right|_{\phi}^{-1} = 8k K(k) \cos 2\pi Q [1 - 4\xi \sin^2 2\pi Q + O(\xi^2)], \quad (15)$$

and $\xi = \exp[-\pi K'(k)/K(k)]$ and $K'(k) = K(\sqrt{1-k^2})$. The first integrals in Eqs. 12 and 13 represents the average over the machine lattice; the second integral represents the average over synchrotron-oscillation period; while the third integral describes particles of different action J' involved in the collision. The integration over J' is performed such that $k(J') \sin 2\pi Q' \approx \sin[\phi(Q, J)/2]$, extending from J_{min} to the bunch edge \hat{J} , with $k(J_{min}) \approx [\sin \phi(Q, J)/2]$. For a round beam with near constant $D/\beta_x^{1/2}$, we have for $I_F(\lambda)$ and $I_D(\lambda)$,

$$I_F = 2g^2 \text{sgn}(\lambda) e^{-(D\gamma\lambda/2\sigma_x)^2} \left\{ 1 - \sqrt{\pi} \|\lambda\| e^{\lambda^2} [1 - \Phi(\lambda)] \right\}$$

$$I_D = g e^{-(D\gamma\lambda/2\sigma_x)^2} \left\{ \sqrt{\pi} (1 + 2\lambda^2) e^{\lambda^2} [1 - \Phi(\lambda)] - 2\|\lambda\| \right\} \quad (16)$$

where Φ is the error function, and $\text{sgn}(\lambda)$ is 1 if $\lambda \geq 0$, and is -1 if otherwise.

Starting from an initial distribution, Eq. 10 can be iterated to yield the time evolution of the longitudinal particle distribution, as shown in Fig. 2. Based on the distribution, evolution of the transverse beam dimension is obtained from Eq. 6. Beam loss through the RF bucket boundary (separatrix) is evaluated from the reduction of the integrated area $\int \Psi(J) dJ$. Typically, the longitudinal distribution under intra-beam scattering is Gaussian-like with zero density at the edge of the RF bucket, as shown in Fig. 2.

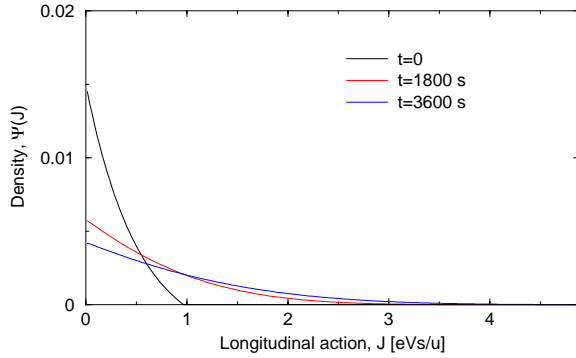


FIGURE 2. Evolution of the longitudinal density distribution under intra-beam scattering during the 1 hour beam experiment at RHIC store. The edge of RF bucket corresponds to 4.9 eV-s/u. The distribution projected on the RF phase ϕ remains Gaussian-like.

Below transition, the dynamical drift term ($F(J)$) typically dominates, leading into energy (heat) transfer between different directions; above transition, the diffusion term ($D(J)$) typically dominates, leading into diffusive growth of beam emittances.

The Fokker-Planck approach was also used to evaluate stochastic cooling efficiency, where the drift term corresponds to coherent cooling and the diffusion term corresponds to incoherent heating [8].

Molecular dynamics and high-density limit

In the case of ultra-fast beam cooling, the density of the cold beam can be exceedingly high. When the Coulomb logarithm approaches 1, the usual Fokker-Planck approximations are no longer valid. Instead, molecular dynamics (MD) methods can be used to evaluate N -body Coulomb interaction under the accelerator environment [11].

Fig. 3 shows the heating rate for a beam at ultra low temperature using the Hamiltonian of Eqs. 1 and 2. In contrary to the scaling of the conventional IBS theory (Eq. 6) shown in the broken line predicting a monotonically increasing heating rate with decreasing temperature (or emittances), the heating rate reduces when the temperature is lowered below $T \approx 1$, which corresponds to the onset of ordering among the particles [10].

RHIC EXPERIMENTS

Beam size rms growth rates were measured and compared with theory in several storage rings including ISR [13], SPS [14], AA [15], and RHIC [16], and the deviations were found to be $< 10 - 20\%$.

The year 2004 dedicated IBS beam experiments in RHIC aimed at three goals: rms beam size growth, debunching beam loss, and longitudinal beam profile evolution. The fully stripped $^{197}\text{Au}^{79+}$ beams were injected

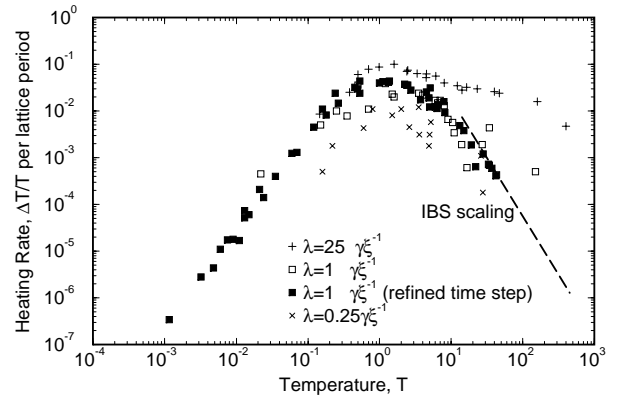


FIGURE 3. Typical heating rates at ultra-low temperature obtained by MD simulation at various line densities λ .

and accelerated to the top energy of 100 GeV/u. The “blue” and the “yellow” ring each contains six bunches at three levels of injected bunch intensities of about $0.8, 0.6,$ and 0.3×10^9 , respectively. In order to distinguish the IBS effects, the counter-circulating beams in the two rings were separated to avoid beam-beam collisions. Irrelevant instrumentations like the tune kickers and Landau-damping cavities were turned off. A single-harmonic, low frequency (28 MHz, $h = 360$, 300 kV peak voltage) RF system was used to confine the beams longitudinally. For a side-by-side comparison, the RF synchronous phase of the blue ring was jumped by about 90 degrees to create hollow longitudinal particle distribution to contrast the Gaussian-like distribution in the yellow ring. In both the horizontal and vertical directions, the particle distribution remains Gaussian-like and transversely coupled.

Using fast ionization profile monitors, the transverse profiles of the beam in the ring were measured. The rms beam emittances were evaluated with the design lattice functions after subtracting the background and fitting to a Gaussian distribution. The wall current monitor was used to measure the longitudinal beam profiles and to evaluate the de-bunching beam loss. A typical measurement lasts for from 0.5 to 1 hour.

Computer simulation was performed with the BBFP (Bunched-beam Fokker Planck) codes [3]. The longitudinal action (J) space was equally divided into bins, and the initial distributions $\Psi(J)$ in action were generated such that their projections on the phase axis ϕ match the measured profiles (Fig. 4). Evolution of $\Psi(J)$ was obtained by iterating Eqs. 10 using time-varying transverse emittance determined by Eq. 6.

A comparison is given in Fig. 5 of the growth of the normalized, 95% vertical emittance for two different intensities (0.6×10^9 and 0.3×10^9 per bunch) of the Gaussian-like bunches in the yellow ring. The simulation is based on fully coupled transverse motion with design

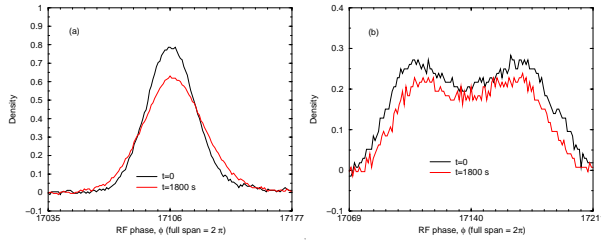


FIGURE 4. Evolution of the longitudinal beam distribution profile measured by the wall current monitor for (a) Gaussian-like and (b) hollow beams.

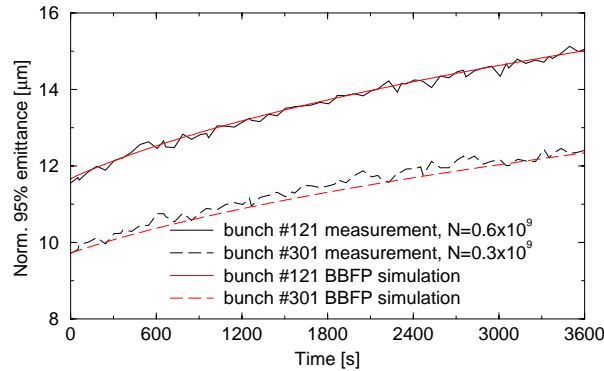


FIGURE 5. Comparison of the growth of vertical emittance between the measurement and simulation for two intensities.

arc FODO lattice of RHIC at the operating tunes.

Fig. 6 compares the de-bunching beam loss between the measurement and simulation for the Gaussian-like and hollow distributions at the initial intensity of about 0.6×10^9 per bunch. Due to the large longitudinal beam size, the loss for the hollow bunch is about 10 times the loss of the un-kicked, Gaussian-like bunch.

Fig. 7 compares the evolution of longitudinal profiles between the measurement and simulation for the Gaussian-like and hollow distributions at the initial intensity of about 0.6×10^9 per bunch. The Gaussian-like

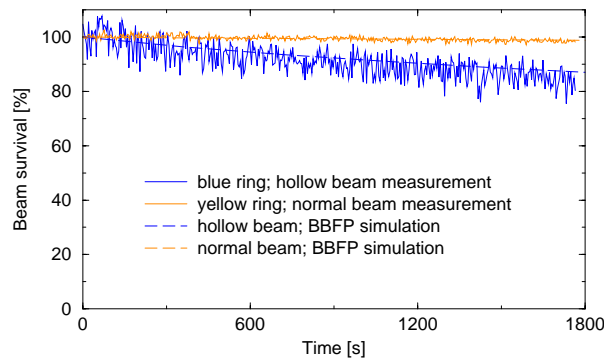


FIGURE 6. De-bunching loss comparison for Gaussian-like (yellow ring) and longitudinal hollow (blue ring) beams.

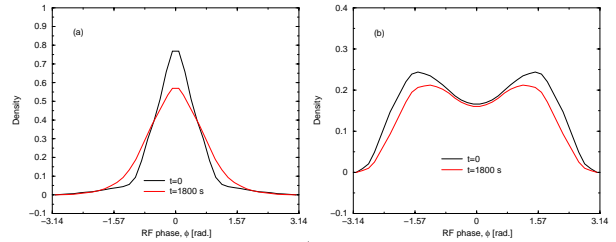


FIGURE 7. Evolution of the longitudinal beam distribution profile simulated with the BBFP codes and projected on the ϕ axis for (a) Gaussian-like and (b) hollow beams.

bunch simply widens its width. On the other hand, the hollow bunch asymptotically approaches a Gaussian shape with its peaks reducing their height faster than the center and with the profile reducing its width over time.

DISCUSSIONS AND SUMMARY

This paper mainly summarizes the development and application of IBS theory in hadron colliders. Calculations include the growth rate of the rms beam emittance using the conventional Gaussian-distribution model, and the distribution function evolution using the Fokker-Planck equations. During the 2004 beam experiments in RHIC, the evolution of beam emittance, the de-bunching beam loss, and the longitudinal beam profiles at storage were measured and compared with the theory for both the Gaussian-like and hollow distributions. The agreement is satisfactory. Future planned RHIC studies include detailed growth-rate dependence on the transverse coupling, the growth rate sensitivity to the average dispersion and dispersion fluctuation of the machine, and the IBS dynamics at injection (positive-mass regime).

We thank M. Blaskiewicz, M. Brennan, R. Connolly, V. Litinenko, T. Roser, T. Satogata, S. Tepikian, J. van Zeijt for many useful discussions.

REFERENCES

1. A. Piwinski, Proc. 9th Int. Conf. on High Energy Acc., Stanford (1974) p. 405
2. J.D. Bjorken, S.K. Mtingwa, Part. Accel., **13** (1983) 115
3. J. Wei, A.G. Ruggiero, BNL, AD/RHIC-81 (1990)
4. V. Lebedev, these proceedings
5. P. Zenkevich, these proceedings
6. M. Martini, CERN PS/84-9 (AA) (1984)
7. G. Parzen, Nucl. Inst. Meth. **A256** (1987) 231
8. J. Wei, A.G. Ruggiero, BNL, AD/RHIC-71 (1990)
9. I. Ben-Zvi, et al, Part. Acc. Conf., Portland (2003) 39
10. J. Wei, H. Okamoto, A.M.Sessler, Phys. Rev. Lett. **80** (1998) 2606
11. J. Wei, X.-P. Li, A.M.Sessler, Phys. Rev. Lett. **73** (1994) 3089
12. J. Wei, Part. Acc. Conf., Washington D.C., (1993) p. 3651
13. K. Hübner, Part. Acc. Conf. (1975) p.1416
14. L.R. Evans, J. Gareyte, Part. Acc. Conf. (1985) p. 2234
15. M. Martini, S. can der Meer, CERN PS/AA/ME/75 (1984)
16. W. Fischer, et al, Euro. Part. Acc. Conf. (2002) p. 236